Progress in Biomaterials (2019) 8:51–63
https://doi.org/10.1007/s40204-019-0110-0

ORIGINAL RESEARCH

Biofabrication and characterization of flavonoid-loaded Ag, Au, Au–Ag bimetallic nanoparticles using seed extract of the plant *Madhuca longifolia* for the enhancement in wound healing bio-efficacy

Mukti Sharma[1] · Saurabh Yadav[1] · Narayanan Ganesh[2] · Man Mohan Srivastava[1] · Shalini Srivastava[1]

Received: 18 November 2018 / Accepted: 12 February 2019 / Published online: 21 February 2019

Abstract

The present communication warrants the presence of significant wound healing bio-efficacy of aq. alc. extract of the seed (49.78%) of the plant *Madhuca longifolia*. A family of seven flavonoid fractions have been ascertained in the seed aq. alc. extract of the target plant using LCMS-8030 analysis. In vivo wound healing parameters (wound area, wound closure, epithelization period, skin breaking strength and hydroxyproline content) have been examined in *Swiss albino* mice models. Statistically significant ($p < 0.001$) enhancement in the wound healing bio-efficacy has been effectively induced using flavonoid-loaded gold: ($M_lf@AuNp_s$), silver: ($M_lf@AgNp_s$), and Au–Ag bimetallic: ($M_lf@Au–AgNp_s$) nanoparticles. Among the biofabricated nano-biomaterials, $M_lf@AgNp_s$ exhibited an exceptional enhancement in the wound healing bio-efficacy (80.33%) attaining almost to the level of reference drug Placentrex (84.02%). All the fabricated nano-biomaterials were thoroughly characterized using UV–Vis, XRD, FE-SEM, TEM, EDX, and DLS. The promising enhancement in the wound healing potential of the nano-biomaterial ($M_lf@AgNp_s$) has been explained based on the cumulative effects of biological and nanotech parameters. The bio-fabricated ($M_lf@AgNp_s$) nano-biomaterials using the plant *M. longifolia* have lustrous prospects for the development of complimentary herbal nanomedicine for scaling-up the wound healing bio-efficacy.

Graphical abstract

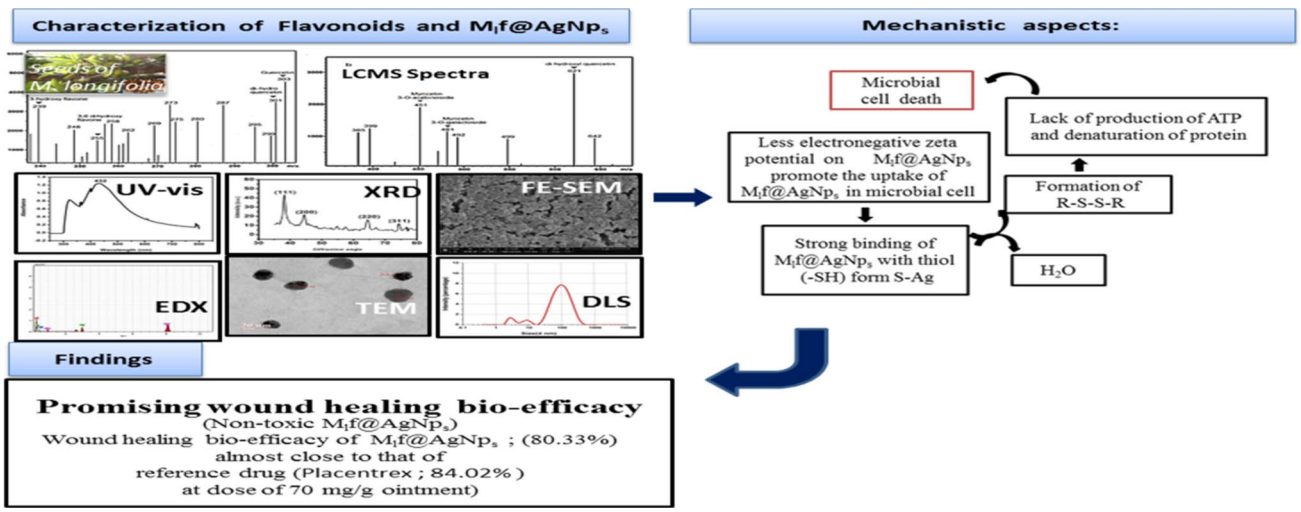

Keywords *Madhuca longifolia* seeds · Flavonoid loaded nano-biomaterials · Characterization of nano-biomaterials · Wound healing activity

Extended author information available on the last page of the article

Abbreviations

$M_lf@AuNp_s$	*Madhuca longifolia* flavonoid-loaded gold nanoparticles
$M_lf@AgNp_s$	*Madhuca longifolia* flavonoid-loaded silver nanoparticles
$M_lf@Au–Ag\ Np_s$	*Madhuca longifolia* flavonoid-loaded gold–silver bimetallic nanoparticles

Introduction

The wound is a rupture in the epithelial integrity of the skin-based structural changes and functions of tissues. Three important phases have been concomitant with the wound healing process (inflammation, cellular proliferation, and remodeling phase). Impaired wound healing results in severe morbidity leading to long hospitalization of patients. There is always demand for treating wounds for minimization of the time taken for healing and to step down the risks of undesired complications (Ahmadi and Adibhesami 2017; Kandhasamy et al. 2017). The use of conventional synthetic drugs over a long time is affiliated with side effects such as coma, hallucinations, kidney, heart, and liver failure (Biondi-Zoccai et al. 2006). The medicinal plants have been borne witnessed as the paramount source of various phytochemicals used for the biogenic synthesis. The use of plant-based nanomaterials has been accounted as a practical approach with improved physico-biochemical properties and functionality (Khoobchandani et al. 2013; Katti 2016). The biogenic nanoparticles have shown promising potential as wound healing agents. The green nanotechnology is an open inquisitive field of research for the enhancement of bio-efficacy and has been exploited in the development of nanodrugs (Murugan et al. 2015; Singh et al. 2018).

Numerous variety of metal nanomaterials are being acquired using gold, zinc, titanium, magnesium, silver, and copper (Sharma et al. 2007; Raliya and Tarafdar 2014; Bhakya et al. 2016; Chung et al. 2017). Among the noble metals, silver and gold have been a focus of interest for pharmacological bio-efficacies (Elia et al. 2014; Fatimah 2016). Silver, in particular, has potent antimicrobial activity including antifungal, anti-oxidant, anti-inflammatory, and wound healing (Kumar et al. 2016). Further, bimetallization can often surpass the enhancement of the catalytic properties of the original single metal, which may not be achieved by monometallic nanoparticles. The bimetallic nanoparticles are likely to exhibit not only additive combination of the properties of two individual metals, but also demonstrate the synergistic effects of the two metals.

Plant-mediated nanoparticles are non-toxic and ecofriendly than chemically synthesized nanoparticles (Ahmed et al. 2016). Considering the rapid blossoming of nanomedicine, particularly in prevention, diagnosis, and treatment of chronic wounds, this innovative technology will be soon on our doorstep.

Recent realization that the plants having particular bio-efficacy should be explored and enhanced for other bonafide activities, have motivated us to enhance anti-inflammatory bio-efficacy of the plant *Madhuca longifolia* using seed extract saponin-loaded Ag nanoparticles (Sharma et al. 2018). In continuation of our work on this plant; exploring wound healing bio-efficacy in the seeds of the plant *M. longifolia*, the present communication reports a facile green synthesis of seed-extracted flavonoid-loaded Ag, Au, and Au–$AgNp_s$ bimetallic nanoparticles, characterization and statistically significant enhancement in wound healing bio-efficacy. The observed highest enhancement in the wound healing bio-efficacy of $M_lf@AgNp_s$ has been ascribed to the inherent antimicrobial property of silver, nanosizing, biological factors responsible for higher uptake, and coating of medicinally important flavonoid on the nanoparticles.

Madhuca longifolia (Sapotaceae family) is grown in hot and damp climates of India. There is century's old belief and observations of the medicinal uses of plant *M. longifolia* for skin-related issues (Mishra and Padhan2013; Sinha et al. 2017). In spite of its wide use over a long period of time, not much scientific approach has been made to study the wound healing activity of this plant at the nanoscale.

Materials and methods

Microwave–ultrasound assisted extraction

The plant seeds were collected from the village of Rajaborari, Madhya Pradesh, India and were identified by Taxonomy Division, Department of Botany, Dayalbagh Educational Institute, Agra, India, where the sample was deposited with the voucher specimen number DEI/DB/DH/2015-073. The defatted seed powder (250 g) was subjected to microwave-assisted extraction (200 W; 20 min; 25 °C) in aq. alc. solution and cooled. The extract was subjected to an ultrasonic bath for 40 min at room temperature, concentrated by rotavapor and dried with purging nitrogen.

Isolation and characterization of flavonoids

The dried fraction of extract (25 g) was subjected to column chromatographic separation (length 120 cm; diameter 4 cm; stationary phase silica gel 125 g) and eluted with $CH_3Cl/CH_3OH/H_2O$ (70:30:1 v/v). After the removal of solvent, a brown mass was acquired. The brown mass fraction was subjected to LCMS-8030 for characterization of the flavonoid compounds. The experimental conditions were as follows: column; C18 column (4.6 mm × 150 mm, 2.5 µm), stationary phase; silica gel, mobile phase; 0.1%

formic acid and 90.9% methanol, N_2 nebulizing gas flow rate; 2 L/min, temp; 40 °C, injection volume; 0.2 µL scanning range (*m*/*z*); 100–1000; wavelength 254 nm followed by 15 min run time. The mass spectrometric analysis was performed in positive ESI mode.

Biofabrication and characterization of bio-nanomaterials

Optimized experimental conditions of biofabricated nanoparticles were as follows: *Madhuca longifolia* flavonoid-loaded gold nanoparticles ($M_lf@AuNp_s$): At pH 5.5, 1 mL of flavonoid fraction (70 mg/mL) was mixed with 5 mL of hydrogen tetrachloroaurate dihydrate solution ($HAuCl_4 \cdot 2H_2O$: 1mM) in a beaker and reaction mixture was subjected to sonication for 20 min at 20 kHz. *Madhuca longifolia* flavonoid-loaded silver nanoparticles ($M_lf@AgNp_s$): At pH 11.5, 1 mL of flavonoid fraction (70 mg/mL) was added with 10 mL of silver nitrate solution (1 mM) in a beaker and reaction mixture was subjected to sonication for 40 min at 20 kHz. *Madhuca longifolia* flavonoid-loaded bimetallic nanoparticles ($M_lf@Au–AgNp_s$): At pH 10, 1 mL of flavonoid fraction (70 mg/mL) was added to 10 mL of hydrogen tetrachloroaurate dihydrate solution ($HAuCl_4 \bullet 2H_2O$:1 mM), followed by the addition of 10 mL of silver nitrate solution (1mM) in a beaker and mixture was subjected to sonication for 40 min at 20 kHz. The formation of $M_lf@AuNp_s$, $M_lf@AgNp_s$, and $M_lf@Au–AgNp_s$ were perceived by the change in color from pale yellow to ruby red, brown and pink, respectively.

The biofabricated nanoparticles were characterized using Ultraviolet/visible spectroscopy (UV–Vis 3000^+ Lab India, India), X-ray diffraction (Bruker AXS D8 Advance, Germany), Field emission scanning electron microscopy (Nova Nano FE-SEM 450, Netherlands), Transmission electron microscopy, Energy dispersive X-ray spectroscopy (Tecnai G2 T 20 ST, Germany), and Dynamic light scattering (Nano ZS90 model Malvern, Germany).

Formulation prior to topical application

Hard paraffin (25 g) and cetostearyl alcohol (25 g) were mixed and heated gently to 60 °C with constant stirring in a water bath to acquire a gel. White soft paraffin (425 g) and wool fat (25 g) were mixed together and allowed to cool. The optimized doses of the selected amount of reference drug, seed extract, flavonoid fraction, and biofabricated nanoparticles were added into per gram of this ointment and gently mixed.

In vivo bioassay (excision and incision wound model)

Male *Swiss albino* mice (weight 25–30 g) were obtained from animal house of Jawaharlal Nehru Cancer and Research Centre Bhopal, Madhya Pradesh and used for the evaluation of in vivo experiments (vide Ethical permission; CPCSEA Registration no. 500/01/9/CPCSEA/2017). The animals were kept at a temperature of 25–28 °C in clean polypropylene cages with 12 h light and dark cycles with proper pellet diet and water ad libitum. The mice were divided into seven groups, having six animals in each group. Group I served as control. Group II was treated with the reference drug (Placentrex; 70 mg/g ointment). The groups III and IV were treated with seed extract and flavonoid fraction at an optimized dose of 70 mg/g ointment. The groups V, VI, and VII were treated with $M_lf@AuNp_s$, $M_lf@AgNp_s$, and $M_lf@Au–AgNp_s$ at an optimized dose of 70 mg/g ointment. The posterior dorsal side hairs of the mice of all the groups were shaved. Animals were anesthetized prior to the creation of wound using the subcutaneous injection of local xylocaine (0.2 mL; 2% w/v). All the treatment groups along with reference drug, seed extract, flavonoids, and biofabricated nano-biomaterials were applied gently to cover the wounded area daily, until complete healing was achieved. In excision model, an area of 100 mm^2 was carefully excised. The percentage of wound closure was calculated from the wound area (Mekonnen et al. 2013). The healing tissues were isolated on the 12th day from all the groups of the mice evaluated for histological investigation. The period of epithelization was calculated (Gutierrez and Vargas 2006) in terms of the number of days required for falling off the dead tissue remnants without any residual raw wound. In incision model, a longitudinal para vertebral incision of 3 cm in length was made deep through the skin. The wounds were closed with interrupted sutures 1 cm apart. The sutures were removed on the 8th day of post-incision and the treatment was continued. The skin breaking strength of the wound was measured on the 10th day after treatment (Kokane et al. 2009) with a tensiometer (Model: XU22DTF, Shanghai Lun Jie Mechanical and Electrical Co. Ltd., China 2000).

Estimation of hydroxyproline content

On the 15th day, a piece of skin from the healed wound area of all the treatment groups was collected and analyzed for hydroxyproline content (Woessner 1961). The tissues (10 mg) were dried in a hot air oven at 60–70°C and hydrolyzed in 6 N HCl (5 mL) at 130 °C for 4 h in a sealed tube. The hydrolyzate was neutralized to pH 7.0, and was subjected to chloramine T oxidation for 20 min, and the reaction was terminated by the addition of 0.4 M perchloric acid (10 mL). The color developed by the addition of Ehrlich

reagent (10 mL) at 60 °C was measured at 557 nm using UV–Vis spectrophotometer.

Statistical analysis

The results were expressed as the mean ± SD of six animals. The data were analyzed by one-way ANOVA followed by Tukey test. The data were considered significant at $p < 0.001$. Statistical analysis was done using Graph Pad Insat 3.0 software.

Results

Presence of flavonoids

LCMS-8030 chromatogram of the column chromatographic fraction of native seed extract scanned in the lower (230–310) and higher (350–700) ranges of *m*/*z*, exhibited the presence of 3-hydroxy flavones (*m*/*z*: 239), 3,6 dihydroxyflavone (*m*/*z*: 255), dihydroquercetin (*m*/*z*: 301), Quercetin (*m*/*z*: 303), Myricetin 3-O-arabinoside (*m*/*z*: 451), Myricetin 3-O-galactoside (*m*/*z*: 481) and dihydroxyl quercetin (*m*/*z*: 621) on the basis of their $[M-H]^+$ mode (Fig. 1a, b).

Characterization of biofabricated nano-biomaterials

UV–Vis spectroscopy

The synthesis of $M_lf@AuNp_s$ and $M_lf@AgNp_s$was carried out at different concentrations (10^{-4}–10^{-2} M) of hydrogen tetrachloroaurate dihydrate and silver nitrate solution keeping the concentration of flavonoid constant (1 mL; 70 mg/mL) as a function of pH (2.5–13.5) in each case. The surface plasmon resonance bands at the concentration (10^{-3}) of $HAuCl_4.2H_2O$ at λ_{max} = 534 nm (pH 5.5) and $AgNO_3$ solution at λ_{max} = 432 nm (pH 11.5) were considered optimum for the biofabrication of $M_lf@AuNp_s$ and $M_lf@AgNp_s$ because of their higher intensity (Fig. 2). The SPR bands at desirable λ_{max} may be ascribed to the coherent oscillation of the electrons in the conduction band of respective gold and silver nanoparticles.

Formation of Au–Ag bimetallic nanoparticles involved simultaneous co-reduction of Au(III) and Ag(I) solution. At pH 4 and 6, initially, a single peak of Au was obtained at characteristic wavelength 510 and 500 nm, respectively. At both the pH values with the passage of time, one more peak of Ag appeared at characteristic wavelength 430 and 420 nm. The delay in the newly generated peak may be attributed to the relatively slow formation of $AgNp_s$, highlighting the assembling of $AgNp_s$ onto the surface of the $AuNp_s$. At pH 8 and 10, a single peak at 470 and 460 nm appeared. However, no change was discerned at further higher pH. The hypsochromic shift from 470 to 460 nm at pH 10 attributed the

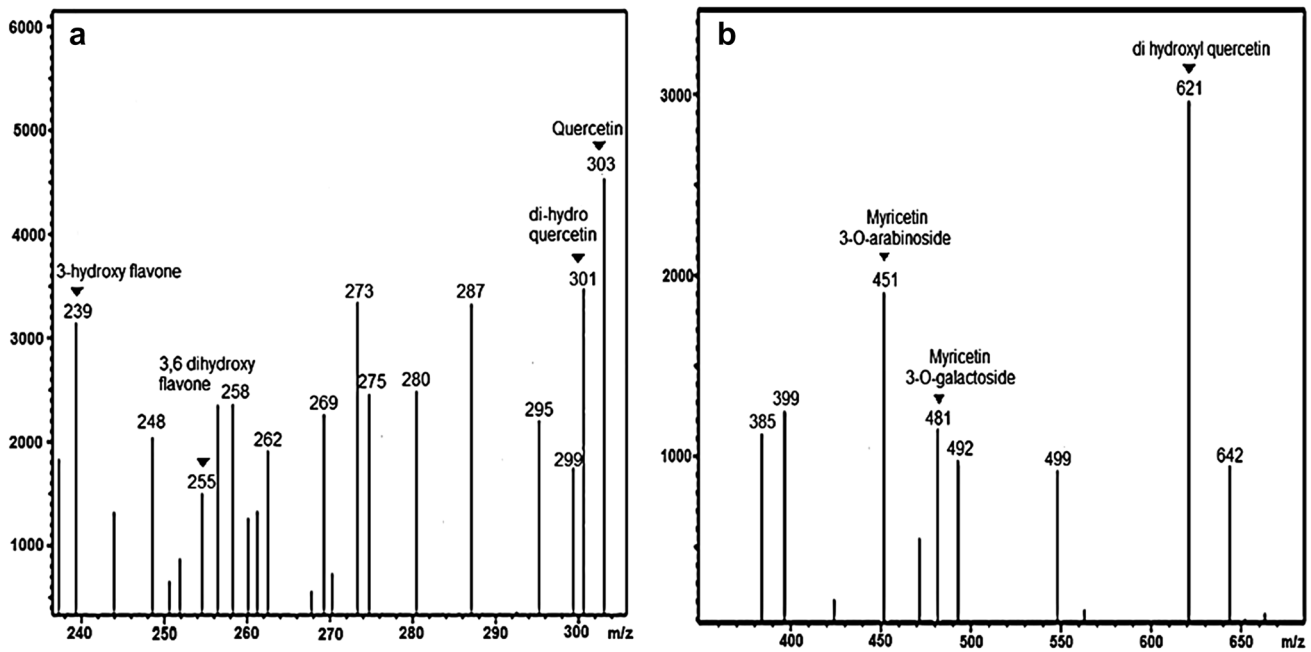

Fig. 1 LCMS chromatogram of seven flavonoids in seed extract of the plant *M. longifolia* in the range **a** 230–310, **b** 350–700

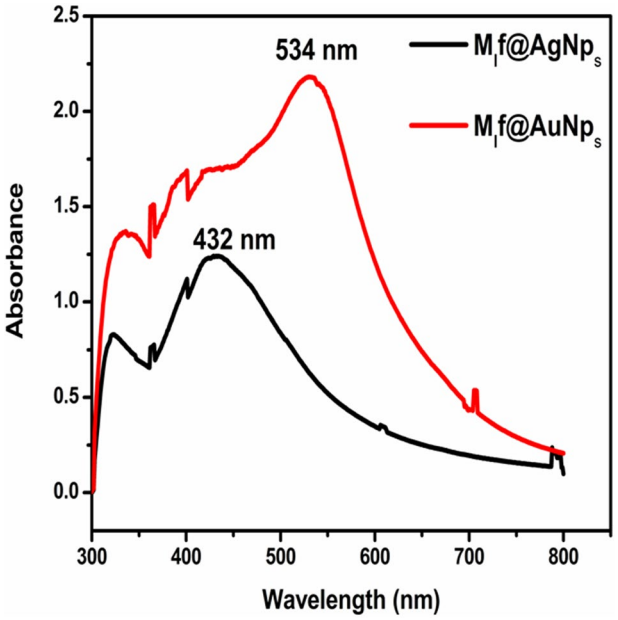

Fig. 2 UV–Vis spectra of $M_lf@AuNp_s$ and $M_lf@AgNp_s$

formation of small-sized and more stable bimetallic nanoparticles (Fig. 3). The observation is in harmony with earlier observation (Ganaie et al. 2016), depicting a single peak of the formation of bimetallic Au–Ag nanoparticles at pH 10. The appearance of wide and shoulder bands in the UV–Vis spectra may be ascertained to the loading of flavonoids on the surface of biofabricated gold, silver, and bimetallic nanoparticles (Shaik et al. 2018). The fact has been supported on the basis of our TEM and DLS studies.

X-ray diffraction

The X-ray diffraction (XRD) profiles of all the biofabricated nanoparticles are depicted in Fig. 4. The three distinct peaks of biofabricated gold and silver nanoparticles were found at 38.18°, 44.39° and 64.57; 38.11° 44.27° and 64.42° diffraction angle, respectively. These peaks correspond to (111) (200) and (220) lattice planes of face-centered cubic structure of gold and silver nanoparticles (JCPDS file 04-0784, 04-0783). The bimetallic Au–$AgNp_s$ had two diffraction peaks at diffraction angles 38.12° and 44.15°. It could be indexed to (111) and (200) having lattice planes of face-centered cubic structure of bimetallic Au–$AgNp_s$. The intensity of the diffraction peak corresponding to (200) crystallographic plane was lower than (111). The 111 plane is known to be more reactive because of its high atom density (Cruz et al. 2010). Some unassigned peaks were also observed due to the crystallization of bio-organic phase (Niraimathi et al. 2013).

FE-SEM and EDX studies

FE-SEM images (Fig. 5a–c) were acquired from drop-coated films of nanoparticles, indicated polydispersed spherical-shaped surface morphology of all the three biofabricated nanoparticles. The desirable signals of gold and silver metals were found in EDX spectra at 2 and 3 keV,

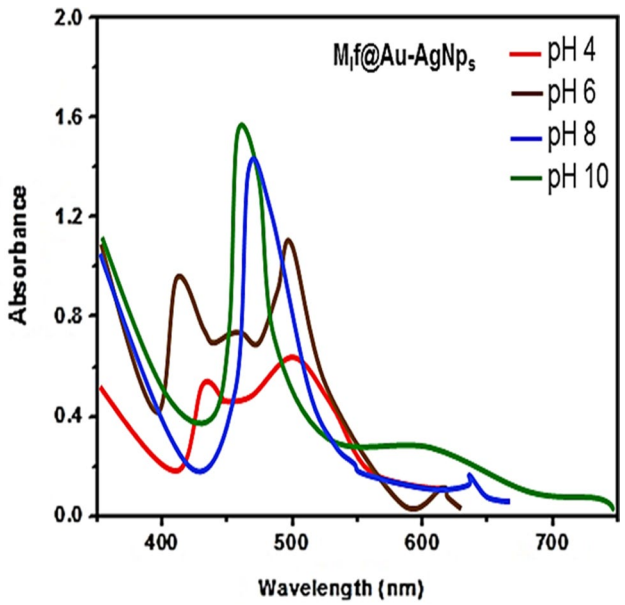

Fig. 3 UV–Vis spectra of $M_lf@Au–AgNp_s$ bimetallic nanoparticles

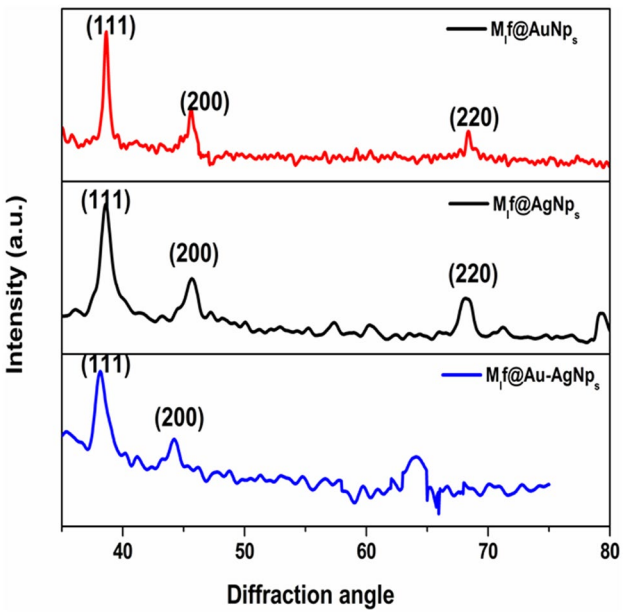

Fig. 4 XRD of $M_lf@AuNp_s$, $M_lf@AgNps$, and $M_lf@Au–AgNp_s$ bimetallic nanoparticles

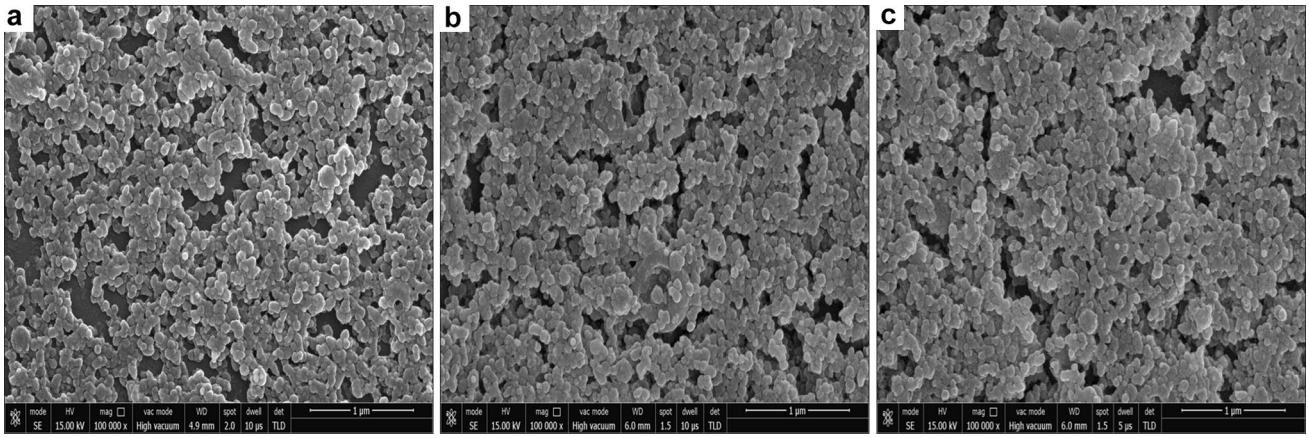

Fig. 5 FE-SEM of M_lf@AuNps, M_lf@$AgNp_s$ and M_lf@Au–$AgNp_s$ bimetallic nanoparticles

respectively (Fig. 6a, b). Both characteristic peaks of Au and Ag at 2 and 3 keV were observed in the EDX spectra of Au–Ag bimetallic nanoparticles (Fig. 6c). The appeared peak of Cu was presumably related with Cu grid on which sample was coated. The peaks of C, O, and N might have initiated from the biomolecules that are adhered to the surface nanoparticles.

TEM and DLS studies

TEM analysis (Fig. 7a–c) also confirmed the spherical shape of all the three biofabricated nanoparticles having diameter range 36–60, 35–50 and 34–66 nm, at the magnification of 300,000×. The appearance of the faint thin layer around the nanoparticles in TEM images was the indication of the coating of secondary metabolites (flavonoids). The average hydrodynamic size (*Z* average given by DLS) of biofabricated nanoparticles, viz M_lf@$AuNp_s$, M_lf@$AgNp_s$, and M_lf@Au–$AgNp_s$ were 74.20, 54.50 and 81.50 nm, respectively. An asymmetric distribution of these nanoparticles was as follows: 50–180, 13–170 and 15–185 nm (Fig. 8a–c). Size of the particles, appeared larger when measured by DLS as compared to the TEM. TEM provides the accurate size of nanoparticles but DLS delivers important information regarding the size distribution of particles. The difference possibly reflects the fact that TEM only measures the physical size while DLS measures the hydrodynamic size of the particles along with the ions attached to the surface and move with nanoparticles in solution (Huang et al. 2007; Cumberland and Lead 2009). The biofabricated nanoparticles M_lf@$AuNp_s$, M_lf@$AgNp_s$, and M_lf@Au–$AgNp_s$ exhibited zeta potentials as− 33.9, −22.5 and − 31.9 mV, respectively (Fig. 9a–c) are quite stable.

In vivo bioassay (excision and incision wound model)

In vivo wound healing bioassay on *Swiss albino* mice was carried out with native seed extract in the various ranges (30, 50, 70 and 80 mg/g ointment). Based on the maximum wound healing potential (wound area, epithelization period, skin breaking strength, and hydroxyproline content in tissues), the dose of native seed extract was optimized (70 mg/g ointment). All the groups except control, dose (70 mg/g ointment) of reference drug, seed extract, flavonoid fraction, M_lf@$AuNp_s$, M_lf@$AgNp_s$, and M_lf@Au–$AgNp_s$ were provided. Table 1 includes various wound healing parameters in the excision and incision wound model at an optimized dose.

Percentage of wound closure in each case was calculated from the reduction in wound area (Fig. 10). The wound closure of seed extract (49.78%) was increased to a level of (59.93%) by flavonoids at the optimum dose (70 mg/g ointment). Interestingly, an increase in the percentage wound closure was induced by all the biofabricated mono and bimetallic nanoparticles at the same dose. The order of the percentage wound closure in different treatment groups was as follows: M_lf@$AgNp_s$ (80.33%) > M_l@Au–$AgNp_s$ (65.97%) > M_lf@$AuNp_s$ (64.37%), highlighting promising wound healing bio-efficacy of M_lf@$AgNp_s$. It seems the combination of silver and gold nanoparticles in the bimetallic M_l@Au–$AgNp_s$ is not enhancing wound healing bio-efficacy greater than M_lf@$AgNp_s$.

Discussion

Since ancient time, seeds of the plant *M. longifolia* are used as folk medicine for skin-associated ailments which indicate the presence of medicinally important secondary metabolites

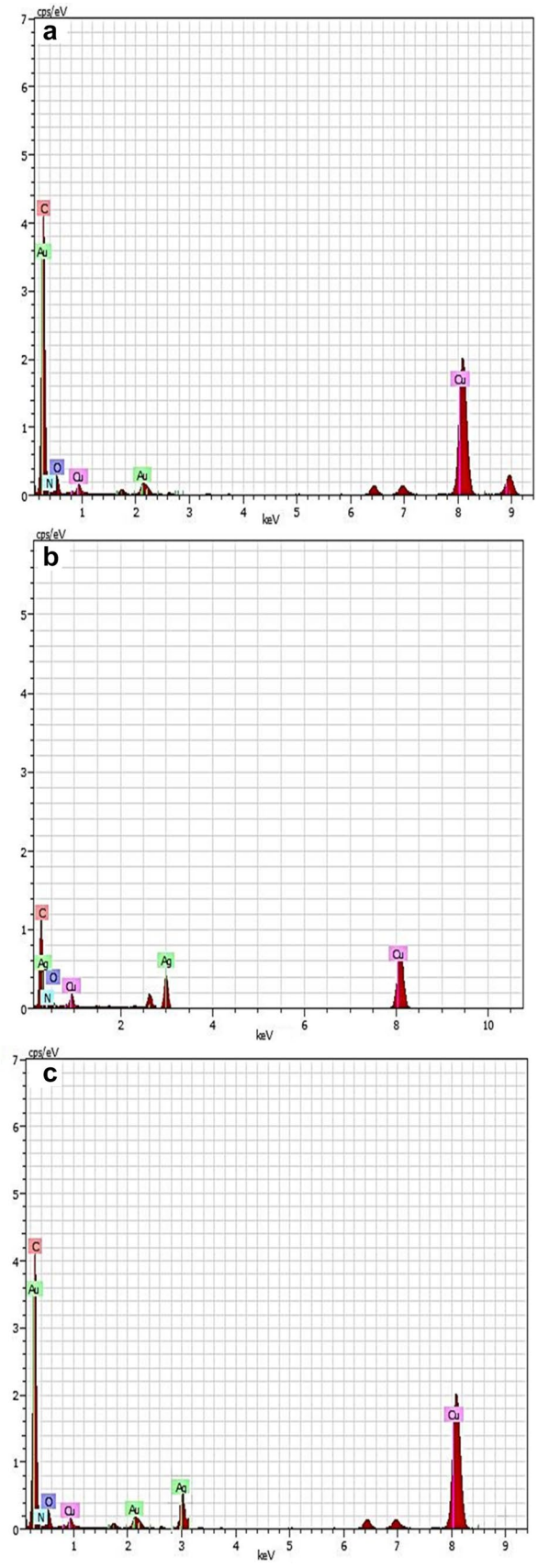

Fig. 6 EDX of $M_lf@AuNp_s$, $M_lf@AgNp_s$ and $M_lf@Au–AgNp_s$ bimetallic nanoparticles

in the plant. Among the secondary metabolites, the polyphenolics and flavonoids have been reported responsible for dealing with skin-related issues (Ambiga et al. 2007; Lodhi and Singhai 2013; Pang et al. 2017). The detailed phytochemical analysis of this plant is lacking. The fact has encouraged us to isolate and characterize flavonoids from the seeds of the plant *M. longifolia*. LCMS-8030 studies of the column chromatographic fraction of native seed extract scanned in the lower (230–310) and higher (350–700) ranges of *m*/*z*, exhibited a family of seven flavonoids (Fig. 1a, b). The strong synergistic reduction potential of flavonoids present in the target plant (seeds) was used for the biofabrication of all the flavonoid-loaded nanoparticles and explored for wound healing bio-efficacy.

A tentative mechanism of reduction of Ag^+ to Ag^0 nanostate form is presented (Scheme 1). The bond dissociation energy (4.6–14.1 kcal/mol) of two –OH groups of catechol moiety of flavonoid is comparatively less (Trouillas et al. 2006) than normal phenolic –OH group (89.0 kcal/mol), facilitating the replacement of $2H^+$ with $2Ag^+$ ions and finally reducing into Ag^0. Therefore, one catechol moiety of flavonoid molecule may reduce two silver ions (two protons per catechol) along with the corresponding quinone moiety. The oxidized quinone being electron deficient in nature may impart additional antioxidant bio-efficacy (free radical scavenging).

The wound healing is a complicated process involving competition in several skin components to permit the repair of damaged tissues. It is promoted by higher cellular uptake of antimicrobial agents enhancing deposition of collagen (increased level of hydroxyproline content), enzymatic interactions, regulation of matrix metalloproteinase enzyme, and pro-inflammatory factors (Shin et al. 2007; Prabhu and Poulose 2012; Caley et al. 2015). The cellular uptake of metal nanoparticles, in addition to the shape and size of nanoparticles, also depends (Zhang et al. 2008) on the extent of binding with the cell membrane (charge difference). Zeta potential values are often used as an indication of the stability of colloidal particles. The absolute values replicate the net electrical charge of the particles of functional groups present on the external surface (Aljabali et al. 2018). The negative value indicated the stability (repulsive barrier) of the nanoparticles preventing the agglomeration of nanoparticles (Patil et al. 2012). The negative potential, in the present case, therefore, might be arising from the loading of negatively charged functional groups (–OH groups of the flavonoids) (Somchaidee and Tedsree 2018). All the biofabricated nanoparticles possess negative charge (zeta potential) in the order: $M_lf@AgNp_s$ (− 22.5 mV) < $M_lf@Au–AgNp_s$ (− 31.5 mV) < $M_lf@AuNp_s$ (− 33.9 mV) indicating the least

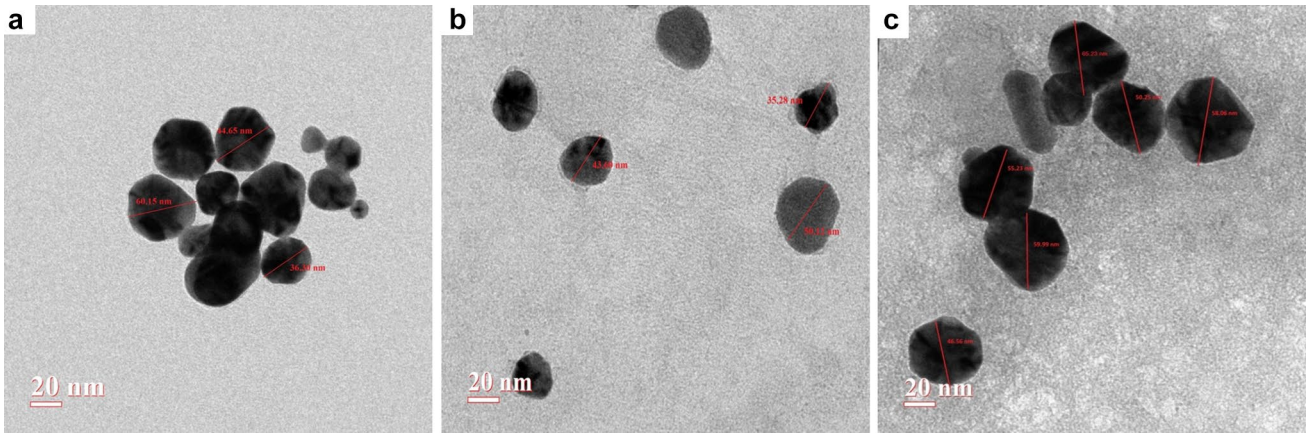

Fig. 7 TEM of $M_lf@AuNp_s$, $M_lf@AgNp_s$and $M_lf@Au–AgNp_s$ bimetallic nanoparticles

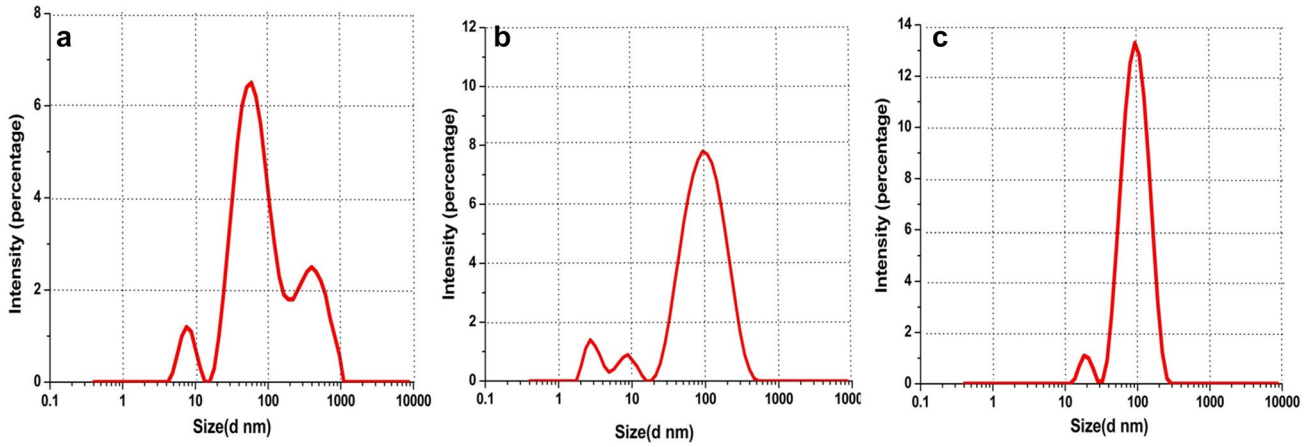

Fig. 8 DLS size distribution curve of $M_lf@AuNp_s$, $M_lf@AgNp_s$ and $M_lf@Au–AgNp_s$ bimetallic nanoparticles

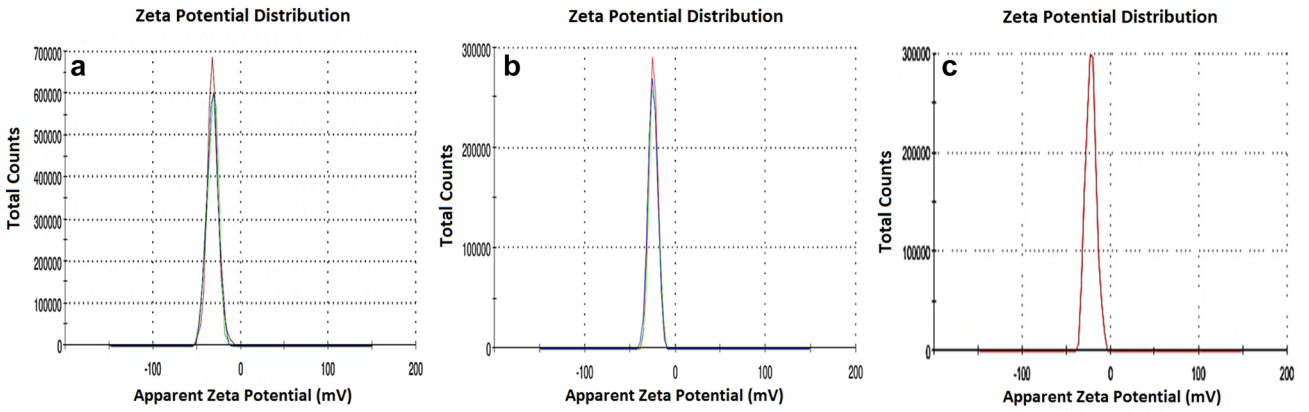

Fig. 9 Zeta potential of $M_lf@AuNps$, $M_lf@AgNp_s$ and $M_lf@Au–AgNp_s$ bimetallic nanoparticles

negative charge on $M_lf@AgNp_s$. The weak negative charge on silver nanoparticles is likely to encounter weak repulsion from strong electronegatively charged cell membrane and result into comparatively higher uptake. The uptake of $M_lf@AgNp_s$ ions is also facilitated by the strong tendency of Ag^+ ions with thiol groups (–SH) of the cell membrane. Such

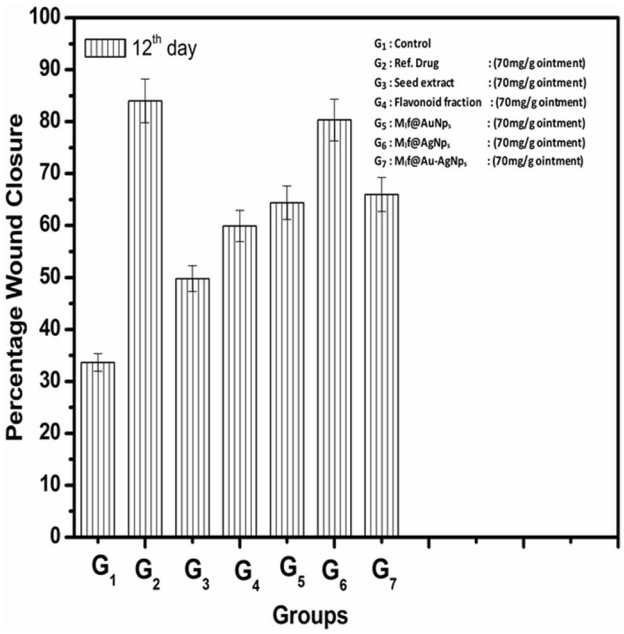

Fig.10 Wound closure % in various treatment groups

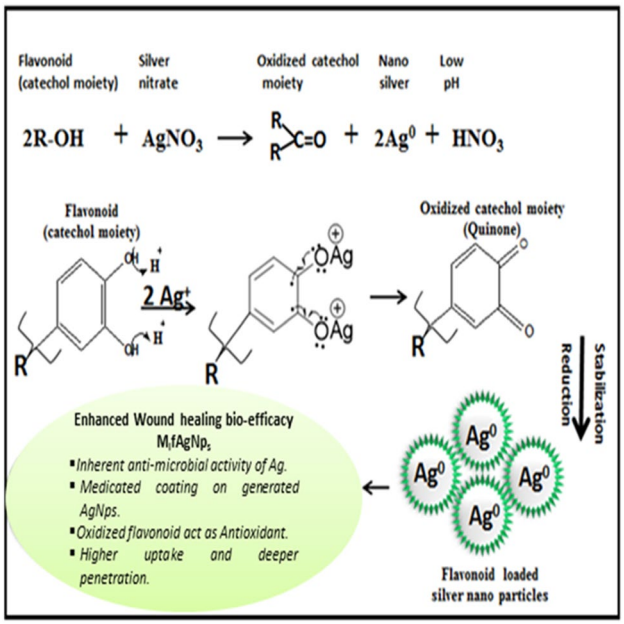

Scheme 1 Proposed chemical reaction of flavonoid fraction with Ag^+ ions rendering the formation of $M_If@AgNp_s$

enzymatic interactions are associated with the generation of ATP formation (Klueh et al. 2000). Silver catalyzes the reaction between the cellular O_2 molecule and the H atom of (–SH) groups forming a disulfide bond (Ag–S–S–Ag) along with the formation of a water molecule instead of being consumed in structure, finally causing cell death (Davies and Etris 1997). Overall, the phenomenon allows accumulation and penetration of nanodrug into living tissues comparatively deeper. Further, a significant increase in the hydroxyproline content in healed tissues confirms the accumulation of collagen level and thus facilitates wound healing bio-efficacy. The enhanced percentage in wound closure (34.03%) compared to flavonoid (59.93%) also supports (Fig. 10) the promising wound healing efficacy of biofabricated $M_If@AgNp_s$ (80.33%).

The skin healing tissues of all the treated groups were isolated on the (12th) day for histological evaluation. In the control group, no recovery appeared in ruptured stratum corneum. The $M_If@AgNp_s$, exhibited trends of good recovery of stratum corneum with the progressively growing a number of well-defined hair follicles (Fig. 11a–c). However, reference drug-treated group revealed sound stratum corneum and fully developed hair follicles with all the three stages. Among the various treatments, $M_If@AgNp_s$ showed faster wound closure rate (80.33%) and epithelization of the wound (18.00 days) (Table 1) with higher wound healing effects as compared to the native seed extract, flavonoid fraction, $M_If@AuN_{ps}$, and M_I f@Au–$AgNp_s$ (Fig. 12a–f).

Conclusions

A stable, simple and eco-friendly technique of biosynthesizing silver ($M_If@AgNp_s$), gold ($M_If@AuNp_s$) and bimetallic gold–silver ($M_If@Au–AgNp_s$) nanoparticles loaded with flavonoids extracted from the seeds of the plant *M. longifolia* were effectively established under ambient conditions. The presence of a family of seven flavonoids in the seed extract of the plant was ascertained using LCMS-8030 analysis. The flavonoids played the major role in the reduction and capping during biofabrication of nanoparticles. All the biofabricated nano-biomaterials were thoroughly characterized. UV–Vis spectroscopy confirmed the surface plasmon resonance band of $M_If@AgNp_s$, $M_If@AuNp_s$, and $M_If@Au–AgNp_s$ at $\lambda_{max} = 432$, 534 and 470 nm, respectively. XRD revealed that all biofabricated nanoparticles were of cubic symmetry. The FE-SEM images reported spherical shapes. The presence of silver, gold and both Au and Ag in the respective nano-biomaterials were confirmed by EDX spectra. TEM analysis reported the accurate size of ($M_If@AgNp_s$: 35–50 nm; $M_If@AuNp_s$: 36–60 nm and $M_If@Au–AgNp_s$: 34–66nm). The surface charge (zeta potential) on the nanoparticles were found $M_If@AgNp_s$ (− 22.5), $M_If@AuNp_s$ (− 33.9), and $M_If@Au–AgNp_s$ (− 31.9). In vivo healing parameters (wound area, wound closure, epithelization period, skin breaking strength and hydroxyproline content) have been examined in *Swiss albino* mice models. Among all biofabricated nanoparticles, $M_If@AgNp_s$ showed significant enhancement (30.40%) in wound healing bio-efficacy compared to native seed extract. The enhanced wound healing

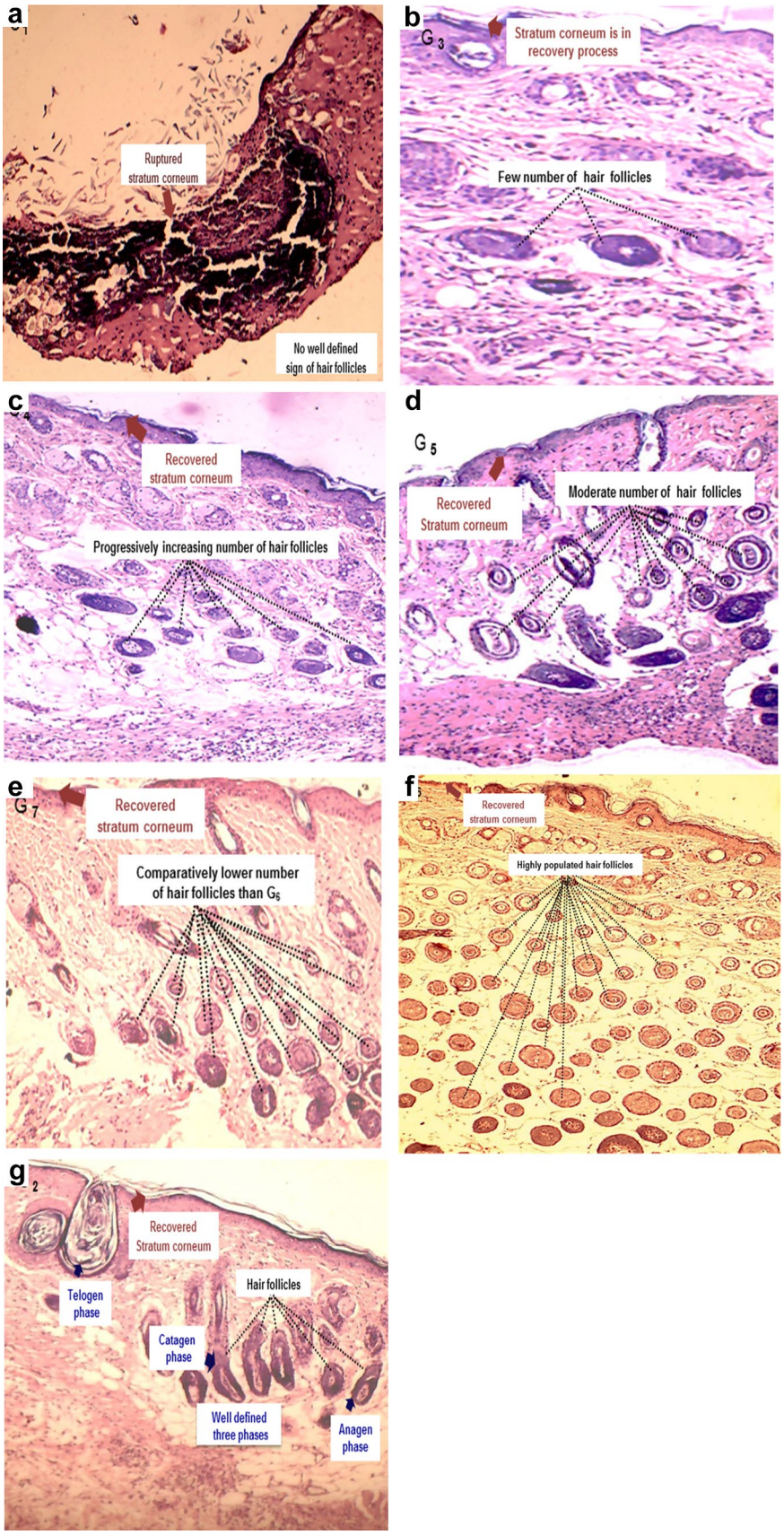

Fig. 11 T.S. of skin: **a** control group, **b** seed extract, **c** flavonoid content, **d** $M_If@AuNp_s$, **e** $M_If@Au–AgNp_s$, **f** $M_If@AgNp_s$, **g** reference drug at optimum dose 70 mg/g ointment, demonstrating progressive skin healing in terms of number of hair follicles and recovered stratum corneum

Table 1 Effect of various treatments on wound healing parameters in the excision and incision wound models at an optimized dose

Groups optimized dose (70 mg/g ointment) except for control	Wound area (mm^2) excision model	Epithelization period (days)	Breaking strength (g) incision model	Hydroxyproline (mg/g)
	12th day	–	10th day	15th day
1.Control	66.34 ± 1.70	33.00 ± 1.26	272.96 ± 1.30	30.21 ± 1.18
2. Placentrex	15.97*** ± 1.39	15.16*** ± 1.16	653.44*** ±1.05	80.23*** ± 1.44
3. Seed extract	50.63 ** ± 1.02	27.00*** ± 1.67	312.21 ** * ± 1.06	40.22*** ± 0.75
4. Flavonoid fraction	40.06*** ± 1.06	24.50*** ± 1.51	467.43*** ± 1.26	62.45*** ± 1.92
5.$M_If@AuNp_s$	35.62*** ± 1.65	21.33*** ±1.50	612.85*** ±1.80	68.11*** ± 0.77
6.$M_If@AgNp_s$	19.67*** ± 1.08	18.00*** ± 1.41	624.23*** ± 1.30	76.23***± 1.38
7. $M_If@Au–AgNp_s$	34.02***±1.62	21.00*** ±1.50	616.01*** ± 1.55	70.03*** ± 1.42

Each value is the mean ± SD of six mice ($n = 6$) at ***$p < 0.001$

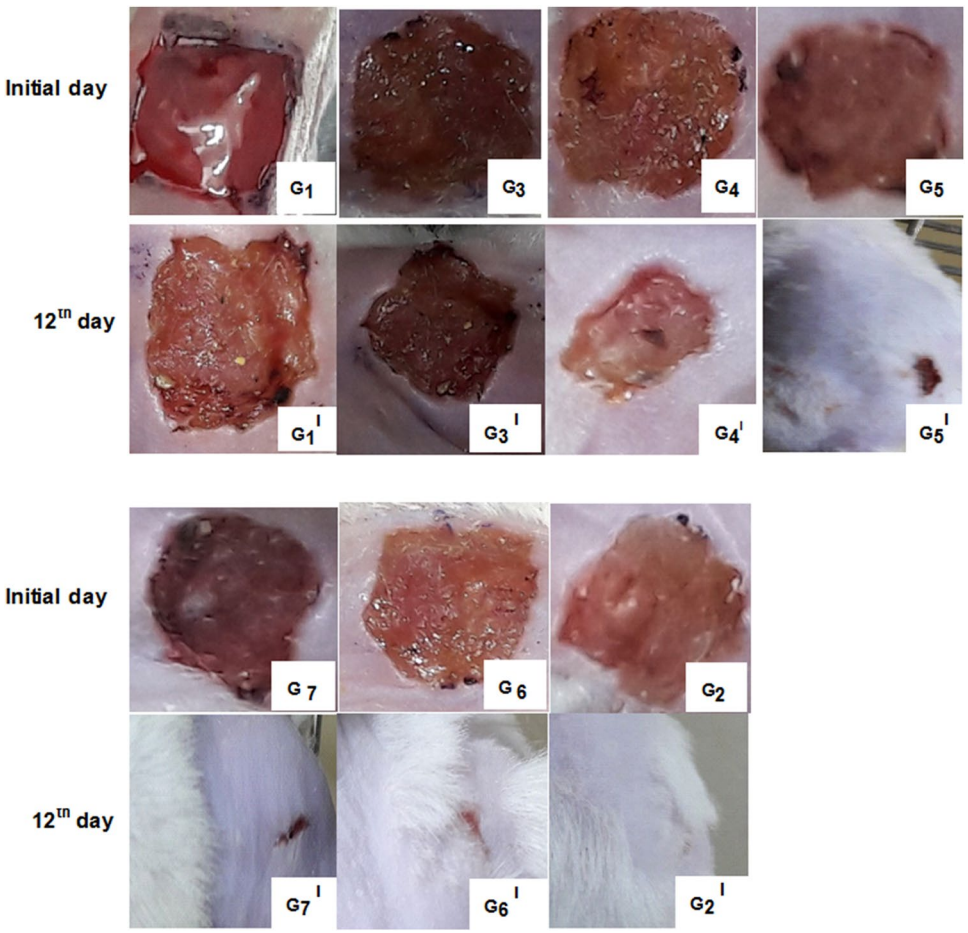

Fig. 12 Photographs of skin on initial day and 12th day: (G_1, G_1^I) control group, (G_3, G_3^I) seed extract, (G_4, G_4^I) flavonoid content, (G_5, G_5^I) $M_If@AuNp_s$, (G_7, G_7^I) $M_If@Au–AgNp_s$, (G_6, G_6^I) $M_If@AgNp_s$, (G_2, G_2^I) reference drug at optimum dose 70mg/g ointment demonstrating progressive decrease in wound size

potential of $M_If@AgNp_s$ was assigned to the inherent antimicrobial property of Ag, zeta potential difference, the large surface area of nanoparticles, and coating of medicinally important flavonoid content on the nanoparticles. The oxidized flavonoids (quinone moiety) being electron deficient also impart additional antioxidant properties. The flavonoid-loaded silver nanoparticles have valuable future and open a novel channel for the development of effective complimentary herbal nanomedicine.

Acknowledgements Authors are thankful to Prof. P.K. Kalra, Director, Dayalbagh Educational Institute, Agra and Prof. Sahab Dass, Head of the Department, for extending all the necessary facilities and motivation to carry out the research. The financial support to Mukti Sharma for this investigation given by the University Grants Commission

(UGC), New Delhi (India) under UGC BSR/Fellowship no. ET/UGC /2136 is gratefully acknowledged.

Conflict of interest Mukti Sharma, Saurabh Yadav, NarayananGanesh, Man Mohan Srivastava, and Shalini Srivastava declare that they have no conflict of interest.

Ethical approval All procedures performed in studies involving animals were in accordance with the ethical standards of the institution (CPCSEA: Committee for the Purpose of Control and Supervision of Experiments on Animals) or practice at which the studies were conducted.

References

Ahmadi M, Adibhesami M (2017) The effect of silver nanoparticles on wounds contaminated with *Pseudomonas aeruginosa* in mice: an experimental study. Iran J Pharm Res 16(2):661–669

Ahmed S, Saifullah Ahmad M, Swami BL, Ikram S (2016) Green synthesis of silver nanoparticles using *Azadirachta indica* aqueous leaf extract. J Radiat Res Appl Sci 9:1–7

Aljabali AAA, Akkam Y, Zoubi MSA, Al-Batayneh KM, Al-Trad B, Alrob OA, Alkilany AM, Benamara M, Evans DJ (2018) Synthesis of gold nanoparticles using leaf extract of *Ziziphus zizyphus* and their antimicrobial activity. Nanomaterials 8:174. https://doi.org/10.3390/nano8030174

Ambiga S, Narayanan R, Gowri D, Sukumar D, Madhavan S (2007) Evaluation of wound healing activity of flavonoids from *Ipomoea carneajacq*. Anc Sci Life 26(3):45–51

Bhakya S, Muthukrishnan S, Sukumaran M, Grijalva M, Cumbal L, Franklin-Benjamin JH, Kumar TS, Rao MV (2016) Antimicrobial, antioxidant and anticancer activity of biogenic silver nanoparticles—an experimental report. RSC Adv 6:81436–81446

Biondi-Zoccai GGL, Lotrionte M, Agostoni P, Abbate A, Fusaro M, Burzotta F, Testa L, Sheiban I, Sangiorgi G (2006) A systematic review and meta-analysis on the hazards of discontinuing or not adhering to aspirin among 50,279 patients at risk for coronary artery disease. Eur Heart J 27(22):2267–2674

Caley MP, Martins VLC, O'Toole EA (2015) Metalloproteinases and wound healing. Adv Wound Care 4:225–234

Chung IM, Rahuman AA, Marimuthu S, Kirthi AV, Anbarasan K, Padmini P, Rajakumar G (2017) Green synthesis of copper nanoparticles using *Eclipta prostrat*a leaves extract and their antioxidant and cytotoxic activities. Exp Ther Med 14:18–24

Cruz D, Fale PL, Mourato A, Vaz PD, Serralheiro ML, Lino ARL (2010) Preparation and physicochemical characterization of Ag nanoparticles biofabricationzed by *Lippia citriodor*a. Colloids Surf B81(1):67–73

Cumberland SA, Lead JR (2009) Particle size distributions of silver nanoparticles at environmentally relevant conditions. J Chromatogr A 1216(52):9099–9105

Davies RL, Etris SF (1997) The development and functions of silver in water purification and disease control. Cat Today 36:107–114

Elia P, Zach R, Hazan S, Kolusheva S, Porat Z, Zeiri Y (2014) Green synthesis of gold nanoparticles using plant extracts as reducing agents. Int J Nanomed 9:4007–4021

Fatimah I (2016) Green synthesis of silver nanoparticle using extract of *Parkia speciosa* Hassk pods assisted by microwave irridation. J Adv Res 7:961–969

Ganaie SU, Abbasi T, Abbasi SA (2016) Rapid and green synthesis of bimetallic Au–Ag nanoparticles using an otherwise worthless weed *Antigonon leptopu*s. J Exp Nanosci 11(6):395–417

Gutierrez R, Vargas S (2006) Evaluation of the wound healing properties of *Acalypha langian*a in diabetic rats. Fitoterapia 77(4):286–289

Huang J, Li Q, Sun D, Lu Y, Su Y, YangX Wang H, Wang Y, Shao W, He N, Hong NJ, Chen C (2007) Biosynthesis of silver and gold nanoparticles by novel sundried *Cinnamomum camphora* leaves. Nanotechnology 18(10):105104–105115

Kandhasamy S, Perumal S, Madhan B, Umamaheswari N, Banday JA, Perumal PT, Santhanakrishnan VP (2017) Synthesis and fabrication of collagen coated ostholamide electrospun nanofiber scaffold for wound healing. Appl Mater Interfaces 9(10):8556–8568

Katti KV (2016) Renaissance of nuclear medicine through green nanotechnology: functionalized radioactive gold nanoparticles in cancer therapy—my journey from chemistry to saving human lives. J Radioanal Nucl Chem 309(1):5–14

Khoobchandani M, Zambre A, Katti K, Lin CH, Katti KV (2013) Green nanotechnology from Brassicaceae: development of broccoli phytochemicals-encapsulated gold nanoparticles and their applications in nanomedicine. Int J Green Nanotechnol 1:1–15

Klueh U, Wagner V, Kelly S, Johnson A, Bryers JD (2000) Efficacy of silver-coated fabric to prevent bacterial colonization and subsequent device-based biofilm formation. J Biomed Mater Res Part B App Biomater 53:621–631

Kokane D, More R, Kale M, Nehete M, Mehendale P, Gadgoli C (2009) Evaluation of wound healing activity of root of *Mimosa pudica*. J Ethnopharmacol 124:311–315

Kumar B, Smita K, Seqqat R, Benalcazar K, Grijalva M, Cumbal L (2016) In vitro evaluation of silver nanoparticles cytotoxicity on hepatic cancer (Hep-G2) cell line and their antioxidant activity green approach for fabrication and application. J Photochem Photobiol B 159:8–13

Lodhi S, Singhai AK (2013) Wound healing effect of flavonoid fraction rich fraction and luteolin isolated from *Martynia annua* Linn. onstreptozotocin induced diabetic rats. Asian Pac J Trop Med 6(4):253–259

Mekonnen A, Sidamo T, Asres K, Engidawork E (2013) In vivo wound healing activity and phytochemical screening of the crude extract and various fractions of *Kalanchoe petitiana A*. Rich (Crassulaceae) leaves in mice. J Ethnopharmacol 145(2):638–646

Mishra S, Padhan S (2013) *Madhuca lonigfolia* (Sapotaceae): a review of Its traditional uses and nutritional properties. IJHSSI. 2(5):30–36

Murugan K, Benelli G, Ayyappan S, Dinesh D, Panneerselvam C, Nicoletti M, Hwang JS, Kumar PM, Subramaniam J, Suresh U (2015) Toxicity of seaweed-synthesized silver nanoparticles against the filariasis vector *Culex quinquefasciatu*s and its impact on predation efficiency of the cyclopoid crustacean mesocyclops-slongisetus. Parasitol Res 114(6):2243–2253

Niraimathi KL, Sudha V, Lavanya R, Brindha P (2013) Biosynthesis of silver nanoparticles using *Alternanthera sessilis* (Linn.) extract and their antimicrobial, antioxidant activities. Colloids Surf B 102:288–291

Pang Y, Zhang Y, Huang L, Xu L, Wang K, Wang D, Guan L, Zhang Y, Yu F, Chen Z, Xie X (2017) Effects and mechanisms of total flavonoid fractions from *Blumea balsamifera* (L.) DC. on skin wound in rats. Int J Mol Sci 18(12):2766. https://doi.org/10.3390/ijms18122766

Patil SV, Borase HP, Patil CD, Salunke BK (2012) Biosynthesis of silver nanoparticles using latex from few euphorbian plants and their antimicrobial potential. Appl Biochem Biotechnol 167:776–790

Prabhu S, Poulose EK (2012) Silver nanoparticles: mechanism of antimicrobial action, synthesis, medical applications, and toxicity effects. Int Nano Lett 2(32):1–10

Raliya R, Tarafdar JC (2014) Biosynthesis and characterization of zinc, magnesium and titanium nanoparticles: an eco-friendly approach. Int Nano Lett. https://doi.org/10.1007/s40089-014-0093-8

Shaik MR, Khan M, Kuniyil M, Al-Warthan A, Alkhathlan HZ, Siddiqui MRH, Shaik JP, Ahamed A, Mahmood A, Khan M, Adil SF (2018) Plant-extract-assisted green synthesis of silver nanoparticles using *Origanum vulgare* L. extract and their microbicidal activities. Sustainability 10:913. https://doi.org/10.3390/su10040913

Sharma NC, Sahi SV, Nath S, Parsons JG, Gardea-Torresde JL, Pal T (2007) Synthesis of plant-mediated gold nanoparticles and catalytic role of biomatrix-embedded nanomaterials. Environ Sci Technol 41(14):5137–5142

Sharma M, Yadav S, Srivastava MM, Ganesh N, Srivastava S (2018) Promising anti-inflammatory bio-efficacy of saponin loaded silver nanoparticles prepared from the plant Madhuca longifolia. Asian J Nanosci Mat 1(4):244–261

Shin SH, Ye MK, Kim HS, Kang HS (2007) The effect of nano-silver on the proliferation and cytokine expression by peripheral blood mononuclear cells. Int Immunopharmacol 7:1813–1818

Singh J, Mehta A, Rawat M, Basu S (2018) Green synthesis of silver nanoparticles using sun dried tulsi leaves and its catalytic application for 4-nitrophenol reduction. J Environ Chem Eng 6:1468–1474

Sinha J, Singh V, Singh J, Rai AK (2017) Phytochemistry, ethnomedical uses and future prospects of Mahua (*Madhuca longifolia*) as a food: a review. J Nutr Food Sci 7:573. https://doi.org/10.4172/2155-9600.1000573

Somchaidee P, Tedsree K (2018) Green synthesis of high dispersion and narrow size distribution of zero-valent iron nanoparticles using guava leaf (*Psidium guajava* L) extract. Adv Nat Sci Nanosci Nanotechnol. https://. https://doi.org/10.1088/2043-6254/aad5d7

Trouillas P, Marsal P, Siri D, Lazzaroni R, Duroux JL (2006) A DFT study of the reactivity of OH groups in quercetin and taxifolin antioxidants: the specificity of the 3-OH site. Food Chem 97:679–688

Woessner JF (1961) The determination of hydroxyproline in tissue and protein samples containing small portion of this imino acid. Arch Biochem Biophys 193:440–447. https://doi.org/10.1080/21688370.2015

Zhang Y, Chen Y, Wang T, Zhou J, Zhao Y (2008) Synthesis and magnetic properties of nonporous Co_3O_4 nanoflower. Microporous Mesoporous Mater 114:257–265

Affiliations

Mukti Sharma[1] · Saurabh Yadav[1] · Narayanan Ganesh[2] · Man Mohan Srivastava[1] · Shalini Srivastava[1]

✉ Shalini Srivastava
dei.shalinisrivastava@gmail.com

[1] Department of Chemistry, Faculty of Science, Dayalbagh Educational Institute, Agra 282005, India

[2] Jawaharlal Nehru Cancer Hospital and Research Centre, Bhopal 462001, India